



ALMA MATER STUDIORUM
UNIVERSITÀ DI BOLOGNA

ARCHIVIO ISTITUZIONALE
DELLA RICERCA

Alma Mater Studiorum Università di Bologna
Archivio istituzionale della ricerca

Probing intra- and inter-molecular interactions through rotational spectroscopy: The case of the odorant 2'-aminoacetophenone and its 1:1 water and neon complexes

This is the final peer-reviewed author's accepted manuscript (postprint) of the following publication:

Published Version:

Probing intra- and inter-molecular interactions through rotational spectroscopy: The case of the odorant 2'-aminoacetophenone and its 1:1 water and neon complexes / Salvitti G.; Blanco S.; Lopez J.C.; Melandri S.; Evangelisti L.; Maris A.. - In: THE JOURNAL OF CHEMICAL PHYSICS. - ISSN 0021-9606. - STAMPA. - 157:14(2022), pp. 144303.144303-144303.144314. [10.1063/5.0117516]

Availability:

This version is available at: <https://hdl.handle.net/11585/902400> since: 2024-01-23

Published:

DOI: <http://doi.org/10.1063/5.0117516>

Terms of use:

Some rights reserved. The terms and conditions for the reuse of this version of the manuscript are specified in the publishing policy. For all terms of use and more information see the publisher's website.

This item was downloaded from IRIS Università di Bologna (<https://cris.unibo.it/>).
When citing, please refer to the published version.

(Article begins on next page)

This is the final peer-reviewed accepted manuscript of:

Salvitti, G., Blanco, S., Lopez, J.C., Melandri, S., Evangelisti, L. and Maris, A., 2022. Probing intra-and inter-molecular interactions through rotational spectroscopy: The case of the odorant 2'-aminoacetophenone and its 1: 1 water and neon complexes. The Journal of Chemical Physics, 157(14).

The final published version is available online at: <https://doi.org/10.1063/5.0117516>

Terms of use:

Some rights reserved. The terms and conditions for the reuse of this version of the manuscript are specified in the publishing policy. For all terms of use and more information see the publisher's website.

This item was downloaded from IRIS Università di Bologna (<https://cris.unibo.it/>)

When citing, please refer to the published version.

Probing intra- and inter-molecular interactions through rotational spectroscopy: The case of the odorant 2'-aminoacetophenone and its 1:1 water and neon complexes

G. Salvitti,^{1,a)} S. Blanco,^{2,b)} J. C. López,^{2,b)} S. Melandri,^{1,3,4,a)} L. Evangelisti,^{3,4,5,a)} and A. Maris^{1,3,a1c)}

AFFILIATIONS

¹ Department of Chemistry "Giacomo Ciamician," University of Bologna, I-40126 Bologna, Italy

² Department of Physical Chemistry and Inorganic Chemistry, IU-CINQUIMA, University of Valladolid, E-47011 Valladolid, Spain

³ Interdepartmental Centre for Industrial Aerospace Research (CIRI Aerospace), University of Bologna, I-47121 Forlì, Italy

⁴ Interdepartmental Centre for Industrial Agrifood Research (CIRI Agrifood), University of Bologna, I-47521 Cesena, Italy

⁵ Department of Chemistry "G. Ciamician," University of Bologna, I-48123 Ravenna, Italy

^{a)} <https://site.unibo.it/freejet/en>.

^{b)} <https://gier.blogs.uva.es/>.

^{c)} Author to whom correspondence should be addressed: assimo.maris@unibo.it

ABSTRACT

The chirped-pulse Fourier transform microwave spectrum of 2'-aminoacetophenone, an aromatic chemical species with odorant properties, has been recorded in the 2–8 GHz frequency range and analyzed, obtaining precise information on the structure of the monomer and its neon and water complexes. The conformation of the monomer is determined by the formation of a resonance-assisted hydrogen bond (RAHB) between the carbonyl and amino groups, which leads to the formation of a bicyclic-like aromatic structure. Accordingly, the cycle formed by the non-covalent bond is preferred to the phenyl ring as the interaction site for neon. In the 1:1 complex, water lies in the molecular plane and forms a strong hydrogen bond with the carbonyl group coupled to an ancillary interaction with the methyl group, leaving the intramolecular RAHB unchanged. The experimental findings are supported by atoms in molecules and symmetry-adapted perturbation theory, which allowed for determining the hydrogen bond and intermolecular interaction energies, respectively.

I. INTRODUCTION

The consciousness of the pivotal role played by non-covalent interactions (NCIs) in chemistry, material science, and biological processes, such as drug–receptor and protein–ligand recognition interactions, and protein folding, has increased in the scientific community over time. Indeed, modern chemistry is now highly focused on the understanding of these kinds of interactions. A chemical interaction is driven by a specific molecular shape and charge distribution, and such properties can be determined in the isolated gas phase by microwave spectroscopy, complemented

by quantum chemical calculations. In this work, we report the rotational spectrum of 2'-aminoacetophenone (2AA from now on) and its weakly bound complexes with neon (2AA·Ne) and water (2AA·W), recorded by means of the chirped-pulse-Fourier transform microwave (CP-FTMW) spectrometer¹ and analyzed with the support of quantum mechanical calculations.

2AA is a volatile, naturally occurring compound with a strong grape-like odor as its main feature. It is the key odorant of some kinds of grapes,² and, over a threshold, it is responsible for the "untypical aging flavor" in white wines.^{3,4} It is also present in several other food compounds, such as milk.⁵ Its strong odor plays an

important role in animals' social behavior as well: for instance, it has been found in urine and fecal material of both mammals (i.e., foxes⁶ and ferrets⁷) and not mammals (i.e., honeybees⁸), where it contributes to sex and individual recognition, and regulates aggressive behaviors inside the social group. Another interesting aspect is its nature as a metabolite of *Pseudomonas aeruginosa*—a ubiquitous, opportunistic human pathogen. The release of 2AA in the food where the bacterium is present enhances the odor of the food and facilitates attraction for several species of flies; this way the bacterium disseminates into other organisms.⁹ This aspect makes 2AA a promising breath biomarker for the detection of the *Pseudomonas aeruginosa* infections in human lungs cystic fibrosis for which the bacterium is responsible.¹⁰ Since olfaction is a very mysterious sense, and even today the mechanism of chemical identification of odorants by olfactory receptors is a matter of intense debate,¹¹ disclosing odorants' structure, flexibility, and ability to form intra- and inter-molecular NCIs could be an important starting point in understanding, modeling and clarifying the unknown aspects of the structure-odor relationship.

From the physical and chemical points of view, 2AA offers a great opportunity to probe NCIs of different nature, since it has three different sites that could be involved in non-covalent interactions: the acetyl group, the amino group, and the aromatic electron π cloud. The acetyl and amino groups can be involved in hydrogen bond (HB) interactions, acting mainly as proton withdrawing sites, and also as proton donors, whereas the aromatic ring can be involved in different NCIs, such as the π - π stacking, OH- π , NH- π , cation or anion- π interactions,¹² as well as rare gas- π interactions.¹³ By choosing water and neon as ligands, we investigate the intrinsic ability of 2AA to coordinate through both HB and van der Waals interactions.

II. EXPERIMENTAL DETAILS

Commercial samples of 2AA (C_8H_9NO , IUPAC 1-(2-aminophenyl)ethan-1-one, melting point 293 K and boiling point 343–341 K) and $H_2^{18}O$ were used without further purification. The spectrum was recorded in the frequency range of 2–8 GHz using a chirped-pulse-Fourier transform microwave spectrometer (CP-FTMW)¹ described elsewhere.¹⁴ The supersonic jet was generated by the expansion of Ne at backing pressure $P_b \approx 2$ –5 bar through a 0.8 mm diameter, pulsed heating nozzle, with molecular pulses of 900 μs duration. 2AA was held in a reservoir placed at the nozzle and heated at 343 K. When needed, a reservoir with water was inserted in the gas line just before the nozzle. The spectra were recorded in steps of 2 GHz. Chirp pulses of 4 μs were created by an arbitrary waveform generator and amplified to 20 W. The polarization signal was radiated from a horn antenna in a direction perpendicular to that of the expanding gas. A molecular transient emission spanning 40 μs is then detected through a second horn antenna, recorded with a digital oscilloscope and Fourier-transformed to the frequency domain. The accuracy of frequency measurements is estimated to be better than 10 kHz, but given the signal-to-noise ratio of some of the observed lines in the fits, these were given estimated measurement errors of 15 kHz, except for overlapped lines for which it was increased to 30 kHz. Measurements of the spectra were done using the AABS package¹⁵ available, as well as many other useful applications, on the PROSPE

website.¹⁶ The rotational transition lines have been assigned and fitted using the CALPGM program suite.¹⁷

III. COMPUTATIONAL DETAILS

Minima on the conformational potential energy surface (PES) were determined by geometry optimization and subsequent evaluation of the Hessian matrix using the GAUSSIAN 16¹⁸ software package (G16, Rev. A.03).¹⁸ Preliminary calculations applied density functional theory (DFT) through the Becke, three-parameter, Lee–Yang–Parr (B3LYP) hybrid density functional theory,^{19,20} corrected by the D3 version of Grimme's empirical dispersion with Becke–Johnson damping D3(BJ)^{21,22} and combined with the valence triple-zeta quality Karlsruhe polarized type basis set (def2-TZVP).²³ Subsequently, selected cases were further investigated at the *ab initio* level through Møller–Plesset second order perturbation theory (MP2),²⁴ in combination with the valence triple-zeta quality Dunning's correlation-consistent, polarized type basis set, augmented with diffuse functions (aug-cc-pVTZ).²⁵ The theoretical electron density distributions were analyzed by means of Bader's quantum theory of atoms in molecules implemented in MULTIFWN program.²⁶ The intermolecular interaction energy has been evaluated through symmetry-adapted perturbation theory (SAPT)²⁷ using a higher order approach (DF-SAPT2+(3) δ MP2/aug-cc-pVTZ//MP2/aug-cc-pVTZ) implemented in the PSI4 package.²⁸ A distributed polarizability model,²⁹ in the form of the computer program RGDMIN,¹⁶ was used to depict the conformational potential energy surface of the complex in spherical coordinates. The 2AA geometry was fixed to the *ab initio* one and the distance (R_{cm}) between the center of mass (cm) of the two subunits was optimized in the full range $\theta = 0^\circ$ – 180° and $\phi = 0^\circ$ – 360° , with steps $\Delta\theta = \Delta\phi = 10^\circ$.

IV. CONFORMATIONAL SPACE

A preliminary DFT investigation of the conformational space of 2AA, performed at the B3LYP–D3(BJ)/def2-TZVP level of calculation, evidenced that two non-equivalent structures of 2AA are possible, depending on the torsion of the acetyl group, as shown in Fig. 1 and reported in Tables S1 and S2 of the [supplementary material](#). The arrangement with the carbonyl group directed toward

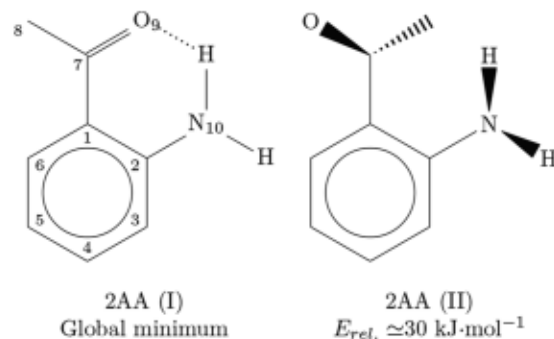


FIG. 1. Sketch and numbering of 2AA's conformers.

the amino group (conformer I), which allows for a CO-HN HB, is by far more stable (33 kJ mol^{-1}) than the one with the methyl group facing the amino group (conformer II). Subsequent *ab initio* optimizations, performed at the MP2/aug-cc-pVTZ level of calculation, confirmed this landscape, lowering the relative energy to 28 kJ mol^{-1} . Due to the sterical hindrance between the methyl and amino groups, conformer II (2AA(II)) is not planar, being the acetyl frame rotated by $162/154^\circ$ (DFT/MP2), with respect to the phenyl ring and the pyramidalization of the amino group $\text{HNHC} = 137/131^\circ$ (DFT/MP2). Differently, due to the HB between the carbonyl and amino groups, an almost planar arrangement is found for conformer I (2AA(I)). In particular, the DFT structure has a perfect C_s symmetry, whereas the *ab initio* data show a slight pyramidalization of the amino group ($\text{HNHC} = 151^\circ$) coupled to a torsion of the acetyl frame ($\text{OC7C1C2} = 1.5^\circ$), being the barrier to planarity, 0.4 kJ mol^{-1} .

The binding between water and 2AA can take place in several ways due to the presence of hydrogen donor and acceptor

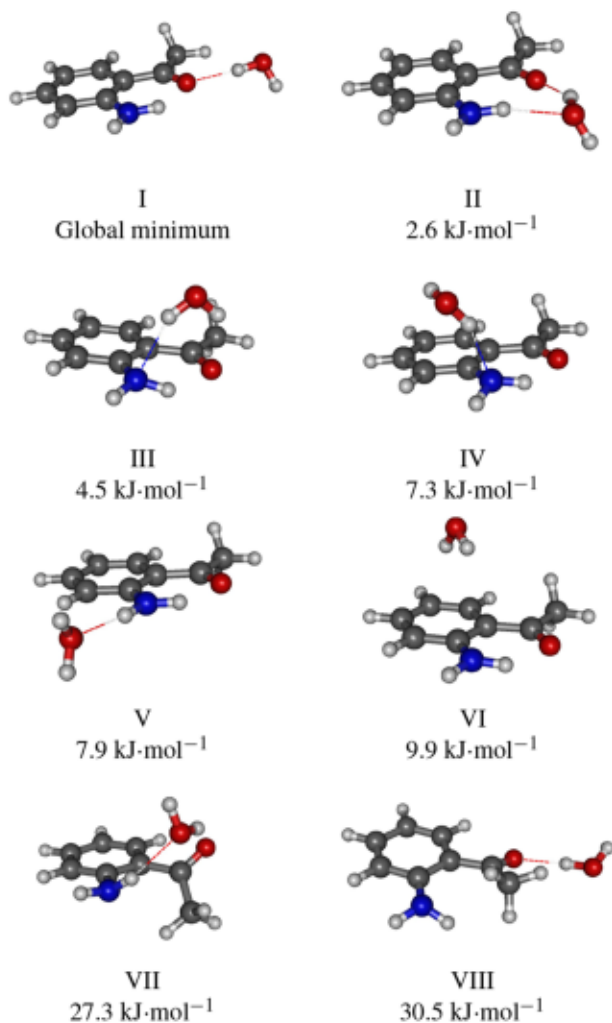


FIG. 2. Structure and relative energy of the most stable conformers of 2AA-H₂O calculated at the B3LYP-D3(BJ)/def2-TZVP level of theory.

sites in both molecules. However, focusing on the most stable form of 2AA, and considering that the stabilization contribution of two inter-molecular interactions should be greater than that of a single interaction, we can hypothesize that the best binding sites are the acetyl basin and the region between the carbonyl and the amino groups. Indeed, both sites allow for a C=O-HOH HB and a secondary interaction involving the water oxygen atom and the hydrogen of the acetyl (conformer I) or amino group (conformer II), respectively. Actually, among all the structures optimized with DFT and shown in Fig. 2, they are the most stable; the acetyl-water arrangement

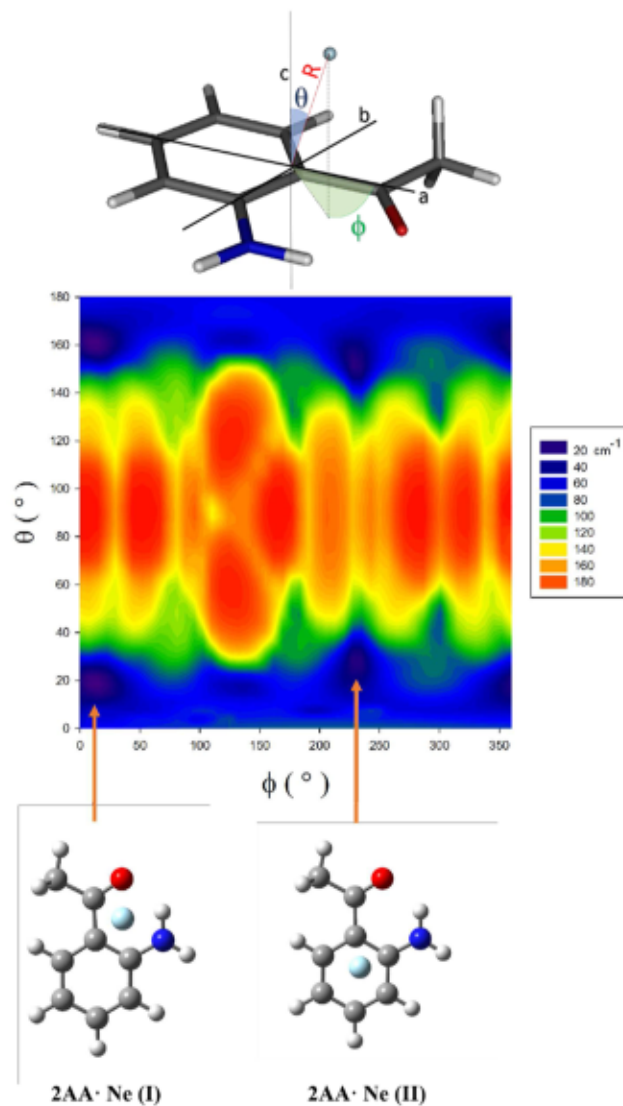


FIG. 3. Conformational potential energy surface of 2AA(I)-Ne. The position of Ne with respect to the center of mass of 2AA is described with spherical coordinates: R is the distance of the Ne atom from the center of mass of the 2AA, θ is the angle that R vector makes with the c -axis of 2AA, and ϕ is the angle between the projection of R in the ab -plane and the a -axis of 2AA. Due to the C_s symmetry of 2AA, the PES is symmetric with respect to $\theta = 90^\circ$.

being favored by about 2.6 kJ mol^{-1} . These two geometries were further optimized at the MP2/aug-cc-pVTZ level of calculation, finding $\Delta E_e \approx 2.4 \text{ kJ mol}^{-1}$.

The calculated structures are given in Tables S3 and S4 of the [supplementary material](#). As for the water complexes of the less stable form of 2AA (conformers VII and VIII), since the intermolecular interactions are the same, the relative energy values reflect the energy difference of the monomers. However, because of the high energy of 2AA (II) and consequently its low concentration in the pre-expansion mixture, low quantities of this form are expected to be formed in the jet, as has been shown in *ortho*-anisic acid-water³⁰ and *ortho*-anisic acid-formic acid.³¹

With regard to complexation with neon, previous studies show that rare gas atoms tend to lie above the molecular ring plane, displaced toward the higher electron density regions.^{32,33} The same trend has been found using a simple distributed polarizability model,²⁹ which allowed to depict a map describing the interaction energy between the neon atom and the most stable form of 2AA. The PES reported in [Fig. 3](#), shows that two non-equivalent and almost isoenergetic minima exist, corresponding to the Ne atom lying above the phenyl ring (conformer II) and above the ring-like structure arising from the intramolecular CO-NH hydrogen bonding (conformer I). Quantum mechanical optimizations suggest a slight preference for the Ne position on the hydrogen bonded ring: $\Delta E_e(\text{DFT}) = 0.14 \text{ kJ mol}^{-1}$ and $\Delta E_e(\text{MP2}) = 0.09 \text{ kJ mol}^{-1}$. The calculated structures are given in Tables S5 and S6 of the [supplementary material](#).

V. ROTATIONAL SPECTRUM

The broadband spectrum of 2AA, recorded in the Ne expansion in the 2–8 GHz frequency range, detected about a thousand transition lines (with a signal-to-noise ratio of at least 3:1). This rich information was disentangled with the support of quantum mechanical computations aimed at the determination of the most stable

molecular structures and their spectroscopic parameters, allowing identifying a plethora of molecular systems. Based on the theoretical spectroscopic constants (reported in [Tables I and II](#)), it has been found that the most intense signals of the spectrum belong to the predicted lowest energy conformers of the 2AA monomer and its 1:1 complexes with water and neon. The rotational transition lines have been assigned by direct diagonalization of the following Hamiltonian using the Watson *S*-reduction and *I'* representation:³⁴

$$\hat{H} = \hat{H}_R + \hat{H}_{CD} + \hat{H}_Q, \quad (1)$$

where \hat{H}_R represents the rigid rotor related to the *A*, *B*, and *C* rotational constants, \hat{H}_{CD} takes into account the centrifugal distortion effect, and \hat{H}_Q is the operator associated with the quadrupole interaction of the ¹⁴N nuclear spin ($I = 1$) with the overall rotation, which leads to a hyperfine structure of the rotational transition lines. The fitted constants are summarized in [Table III](#), whereas the 433 measured transition lines are listed in [Tables S7–S9](#) of the [supplementary material](#). Focusing on the weaker features of the spectrum, several monosubstituted isotopologues were observed in natural abundance, including 2AA(¹³C), 2AA(¹⁵N), 2AA(¹³C)-H₂O, and 2AA-²²Ne. Moreover, additional measurements conducted in the 4–6 GHz region using ¹⁸O enriched water allowed detection of 2AA-H₂¹⁸O. The 247 assigned lines are listed in the SM ([Tables S10–S28](#)), whereas the derived spectroscopic constants are reported in [Tables III–V](#). Several weak lines of the spectrum remained unassigned. Some of them showed a quadrupole hyperfine structure, suggesting that they are related to some 2AA species. Unfortunately, we could not recognize any reliable pattern, even using the HS-AUTOFIT tool, which is appositely designed for automatic fit of crowded spectra.³⁵

TABLE I. Theoretical energy values and spectroscopic parameters at the B3LYP-D3(BJ)/def2-TZVP level of calculation.

	2AA(I)	2AA(II)	2AA-H ₂ O(I)	2AA-H ₂ O(II)	2AA-Ne(I)	2AA-Ne(II)
<i>A</i> /MHz	2250.0	2235.5	2211.0	1588.7	1285.1	1276.3
<i>B</i> /MHz	1211.7	1186.7	603.6	761.4	873.0	824.3
<i>C</i> /MHz	791.4	791.1	476.2	517.4	729.3	761.8
κ	-0.42	-0.45	-0.85	-0.54	-0.48	-0.76
χ_{aa} /MHz	1.36	1.71	1.37	1.68	1.17	1.14
χ_{bb} /MHz	2.80	2.33	2.74	2.30	1.74	2.79
χ_{cc} /MHz	-4.16	-4.04	-4.12	-3.99	-2.91	-3.93
$M_{aa}/\text{u}\text{\AA}^2$	415.51	419.31	835.04	661.20	439.30	440.25
$M_{bb}/\text{u}\text{\AA}^2$	223.05	219.50	226.31	315.57	253.67	223.14
$M_{cc}/\text{u}\text{\AA}^2$	1.56	6.57	2.26	2.54	139.60	172.83
μ_a/D	1.74	1.59	3.76	-1.96	1.71	-1.72
μ_b/D	0.35	-3.70	0.61	0.55	0.03	-0.33
μ_c/D	0.00	0.25	-1.25	-1.18	0.44	0.31
$\mu_{\text{tot}}/\text{D}$	1.78	4.03	4.01	2.36	1.77	1.78
$E_e/\text{a.u.}$	-440.467 968	-440.455 433	-516.943 581	-516.942 579	-569.442 189	-569.442 137
$\Delta E_e/\text{kJ mol}^{-1}$	0	32.90	0	2.63	0	0.14

TABLE II. Theoretical energy values and spectroscopic parameters at the MP2/aug-cc-pVTZ level of calculation.

	2AA(I)	2AA(II)	2AA-H ₂ O(I)	2AA-H ₂ O(II)	2AA-Ne(I)	2AA-Ne(II)
A/MHz	2236.5	2230.6	2206.9	1591.3	1303.4	1302.5
B/MHz	1213.4	1181.0	605.7	756.9	887.3	840.5
C/MHz	790.9	800.5	477.0	516.9	735.2	763.6
κ	-0.42	-0.47	-0.85	-0.55	-0.46	-0.71
χ_{aa}/MHz	1.16	1.38	1.21	1.70	1.05	0.95
χ_{bb}/MHz	2.59	2.07	2.54	2.04	2.12	2.62
χ_{cc}/MHz	-3.75	-3.45	-3.75	-3.73	-3.17	-3.57
$M_{aa}/\text{u}\text{\AA}^2$	414.79	416.34	832.49	663.94	434.61	437.55
$M_{bb}/\text{u}\text{\AA}^2$	224.24	214.99	227.10	313.82	252.79	224.30
$M_{cc}/\text{u}\text{\AA}^2$	1.73	11.58	1.89	3.77	134.94	163.70
μ_a/D	1.54	1.49	3.04	-1.51	1.50	-1.44
μ_b/D	0.70	-3.13	0.90	0.73	-0.24	-0.67
μ_c/D	0.43	0.08	0.05	-0.78	0.87	0.72
$\mu_{\text{tot}}/\text{D}$	1.75	3.47	3.17	1.85	1.75	1.76
$E_e/\text{a.u.}$	-439.408 902	-439.398 332	-515.748 514	-515.747 614	-568.216 184	-568.216 148
$\Delta E_e/\text{kJ mol}^{-1}$	0	27.75	0	2.36	0	0.09

TABLE III. Experimental spectroscopic parameters, S -reduction, and f' -representation.

	2AA	2AA(¹⁵ N)	2AA-H ₂ O	2AA-H ₂ ¹⁸ O	2AA-Ne	2AA- ²² Ne
A/MHz	2234.131 01(8) ^a	2187.546(2)	2196.2855(2)	2195.89(1)	1246.0073(3)	1207.6786(4)
B/MHz	1204.7082(5)	1204.7111(4)	595.930 07(5)	567.8397(1)	835.0648(2)	818.5575(3)
C/MHz	787.067 85(4)	781.2105(3)	470.724 34(5)	453.0133(1)	729.7712(2)	719.1824(3)
D_J/kHz	0.0218(6)	[0.0218] ^b	3.072(3)	3.233(3)
D_{JK}/kHz	0.318(6)	[0.318]	6.18(2)	3.85(2)
d_1/kHz	-0.340(3)	0.461(4)
d_2/kHz	-0.130(2)	0.241(2)
$\frac{3}{2}\chi_{aa}/\text{MHz}$	1.79(1)	...	1.856(1)	[1.856]	1.469(3)	1.362(3)
$\frac{\chi_{bb}-\chi_{cc}}{4}/\text{MHz}$	1.6023(4)	...	1.5879(5)	[1.5879]	0.9244(9)	0.730(1)
σ^2/kHz	4.1	4.5	4.6	3.5	6.3	4.8
N^d	168	...	192	35	73	60
N_{rot}^e	44	9	59	14	24	23
μ_a/D	Y, $J = 2-5^f$	Y, $J = 2-4$	Y, $J = 2-8$	Y, $J = 4-6$	Y, $J = 2-5$	Y, $J = 2-5$
μ_b/D	Y, $J = 1-6$	N	Y, $J = 1-7$	N	N	N
μ_c/D	N	N	N	N	Y, $J = 2-4$	Y, $J = 2-3$
κ	-0.423	-0.398	-0.855	-0.868	-0.592	-0.593
$M_{aa}/\text{u}\text{\AA}^2$	417.6993(1)	417.6973(6)	845.7823(1)	887.725(1)	446.0579(2)	450.8219(3)
$M_{bb}/\text{u}\text{\AA}^2$	224.4043(1)	229.2206(6)	227.8377(1)	227.869(1)	246.4593(2)	251.8914(3)
$M_{cc}/\text{u}\text{\AA}^2$	1.8040(1)	1.8050(6)	2.2686(1)	2.278(1)	159.1395(2)	166.5801(3)
χ_{aa}/MHz	1.192(8)	...	1.237(1)	[1.237]	0.979(2)	2.044(2)
χ_{bb}/MHz	2.608(5)	...	2.557(3)	[2.557]	1.359(3)	0.438(5)
χ_{cc}/MHz	-3.800(5)	...	-3.794(3)	[-3.794]	-2.338(3)	-2.482(3)

^aError in units of the last digit.

^bValues in square brackets are fixed to those of the parent species.

^cStandard deviation of the fit.

^dNumber of hyperfine components in the fit.

^eNumber of rotational components.

^fY/N denotes that such transition type has/has not been observed. Following, the upper J values of the observed transition lines are given.

TABLE IV. Experimental rotational constants of 2AA(¹³C). S-reduction and *I*'-representation. Nuclear quadrupole coupling constants fixed to the values of the parent species.

	A/MHz	B/MHz	C/MHz	σ /kHz ^a	N ^b
C1	2233.701(6) ^c	1204.6435(4)	786.9872(2)	3.4	14
C2	2224.933(5)	1203.8521(3)	785.5645(2)	4.7	20
C3	2226.733(5)	1193.7312(3)	781.4629(2)	4.4	20
C4	2233.045(6)	1185.6530(3)	778.7506(2)	4.2	19
C5	2211.466(5)	1194.8180(3)	780.0314(2)	5.7	18
C6	2213.398(6)	1204.081(3)	784.2114(2)	3.9	16
C7	2233.810(6)	1196.7034(3)	783.6047(2)	6.7	19
C8	2212.969(6)	1187.5288(3)	777.106(2)	3.0	17

^aRoot-mean-square deviation of the fit.

^bNumber of transition lines in the fit.

^cError in units of the last digit.

TABLE V. Experimental rotational constants of 2AA(¹³C)-H₂O. S-reduction and *I*'-representation. Nuclear quadrupole coupling constants and quartic centrifugal distortion constants fixed to the values of the parent species.

	A/MHz	B/MHz	C/MHz	σ /kHz ^a	N ^b
C1	2195.77(2) ^c	595.8252(2)	470.6299(2)	4.8	15
C2	2186.88(2)	595.1309(2)	469.8010(2)	6.4	18
C3	2186.25(3)	591.6318(2)	467.5867(3)	5.1	15
C4	2196.04(2)	588.7033(2)	466.1995(2)	7.0	20
C5	2178.36(2)	591.2192(2)	466.9611(2)	8.6	23
C6	2176.87(2)	594.8974(2)	469.1846(2)	3.8	20
C7	2194.92(2)	595.1857(2)	470.2002(2)	4.8	17
C8	2167.87(2)	593.9326(2)	468.1633(2)	5.5	17

^aRoot-mean-square deviation of the fit.

^bNumber of transition lines in the fit.

^cError in units of the last digit.

VI. STRUCTURE

Straightforward information on the distribution of the *N* atomic masses (m_i) along the axes of the principal axes system (PAS: *a*, *b*, *c*) is provided by the planar moments of inertia, which are related to the rotational constants as follows:

$$\begin{cases} M_{aa} = \sum_{i=1}^N m_i \cdot a_i^2 = \frac{\hbar}{8 \cdot \pi \cdot c} \cdot \left(-\frac{1}{A} + \frac{1}{B} + \frac{1}{C} \right), \\ M_{bb} = \sum_{i=1}^N m_i \cdot b_i^2 = \frac{\hbar}{8 \cdot \pi \cdot c} \cdot \left(+\frac{1}{A} - \frac{1}{B} + \frac{1}{C} \right), \\ M_{cc} = \sum_{i=1}^N m_i \cdot c_i^2 = \frac{\hbar}{8 \cdot \pi \cdot c} \cdot \left(+\frac{1}{A} + \frac{1}{B} - \frac{1}{C} \right), \end{cases} \quad (2)$$

where \hbar is the reduced Planck's constant, and c is the speed of light in vacuum. The experimental and theoretical values are reported in Table I–III, respectively, where the Ray asymmetry parameter ($\kappa = \frac{2B-A-C}{A-C}$)³⁶ is also given.

With regard to 2AA, in agreement with the small value of $M_{cc} = 1.8040(1) \text{ u}\text{\AA}^2$, the atomic masses are mainly located on the *ab* inertial plane. Thus, a C_s symmetry can be hypothesized, where *ab* is the symmetry plane, and only the methyl hydrogen atoms lie out of

plane. However, for such an arrangement a $M_{cc} = 1.59 \text{ u}\text{\AA}^2$ value is expected. The discrepancy between the observed and expected values ($M_{cc}^{\text{obs.}} - M_{cc}^{\text{calc.}} = 0.21 \text{ u}\text{\AA}^2$) suggests the presence of a further out of plane contribution, whose origin can be structural or dynamic. The structural contribution is related to a non-planar distribution of the masses, implying the loss of the symmetry plane. Interestingly, the $M_{cc} = 0.20 \text{ u}\text{\AA}^2$ of aniline (Ph-NH₂),³⁷ whose amino group is not planar, matches quite well the ($M_{cc}^{\text{obs.}} - M_{cc}^{\text{calc.}}$) value of 2AA, suggesting a possible non-planar arrangement of 2AA's amino group. However, molecules are not rigid bodies, and the presence of large amplitude motions can increase or decrease the values of the planar moments of inertia. For instance, despite acetophenone (Ph-COCH₃) being characterized by a C_s geometry,^{38,39} its $M_{cc} = 1.79 \text{ u}\text{\AA}^2$ and $M_{cc}^{\text{obs.}} - M_{cc}^{\text{calc.}} = 0.20 \text{ u}\text{\AA}^2$ values, very similar to those of 2AA, are ascribable to the low torsion energy of the acetyl group, whose fundamental wavenumber determined by far infrared spectroscopy is $\tilde{\nu}_{01} = 49.5 \text{ cm}^{-1}$.⁴⁰ Taking into account both the amino and acetyl contributions, a $M_{cc} = 0.20 + 1.79 = 1.99 \text{ u}\text{\AA}^2$ can be empirically estimated. The lower observed value indicates an overall planarization and stiffening of the bifunctionalized compound. This can intuitively be attributed to the proximity of the acetyl and amino groups, which allows for the formation of a HB between the oxygen and the hydrogen atoms (CO-HN). Upon hydrogen bonding, a weakening of the NH covalent bond is usually observed, which corresponds to a lowering of the corresponding stretching frequency. Accordingly, gas phase infrared data (publicly available at the NIST Chemistry WebBook website)⁴¹ show a 55 cm^{-1} red shift of the NH stretching fundamental in going from aniline (3413 cm^{-1}) to 2AA (3358 cm^{-1}). The lack of observation of μ_c -type transition lines in the rotational spectrum further supports a planar geometrical arrangement of the heavy atoms—thus a C_s molecular symmetry. Moreover, we notice that the out of plane quadrupole coupling constant of 2AA ($\chi_{cc} = -3.800(5) \text{ MHz}$) is very close to that of formamide ($\chi_{cc} = -3.8413(6) \text{ MHz}$ ⁴² or $-3.854(5) \text{ MHz}$ ⁴³). Interestingly, the planar structure of amide groups is explained by a resonance mechanism between the neutral and the zwitterionic forms.⁴⁴ Despite the fact that in 2AA the amine group is not connected to the carbonyl C7 atom (as in amides), thanks to the presence of the phenyl group, a zwitterionic resonant structure can be written also for 2AA (Fig. 4). Considering the ring arising from the formation of the CO-HN HB and, thus, the presence of six *p*-type electrons (the N lone pair and the C1 = C2 and C7 = O π -type electrons, see Fig. 1 for numbering), an additional stabilizing contribution due to the delocalization of the system of conjugated double bonds can be hypothesized. This mechanism of synergistic interplay

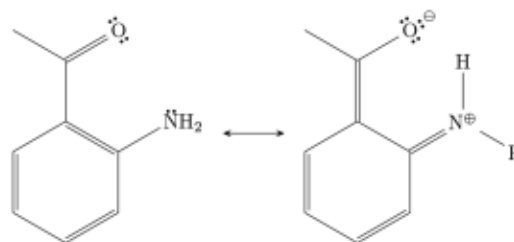


FIG. 4. Neutral and zwitterionic forms of 2AA.

of resonance and HB formation has been defined resonance-assisted hydrogen bonding (RAHB) by Gilli *et al.*⁴⁵ It is worth noting that for the analogous molecule anthranilic acid or *ortho*-aminobenzoic acid, electronic and infrared spectroscopy studies evidenced that an intramolecular hydrogen-atom dislocation from nitrogen to oxygen takes place upon electronic excitation.^{46–48}

As concerns the molecular complexes, looking at the planar moments of inertia, it is evident that the main variations concern M_{aa} (+428 uÅ²) for the water complex and M_{cc} (+157 uÅ²) for the neon one, consistent with a water molecule lying along the *a* axis of 2AA and the neon atom above the *ab* symmetry plane of the monomer. A more precise information on the atoms' positions from rotational constants is achieved using Kraitchman's equations,⁴⁹ which, based on the assumption that different isotopologues share the same geometry, yield the absolute values of the coordinates of the substituted atom in the PAS of the unsubstituted species. The substitution atom coordinates (r_s), derived by Kraitchman's method for the three species, are reported in Table VI and visualized in Fig. 5 in the form of small spheres superimposed onto the theoretical structures. The sign of the r_s coordinates (not directly determinable from the method) was inferred by comparison with the theoretical equilibrium coordinates (r_e , Tables S1–S6 of the [supplementary material](#)). A good agreement between the r_e and r_s structures is evident, and the binding of the water molecule to the acetyl group is confirmed.

It is important to point out that the position of the neon atom can be determined by comparison of the two sets of coordinates obtained by substitution of a dummy atom of zero mass with ²⁰Ne and substitution of ²⁰Ne with ²²Ne. Use of the first set provides the coordinates of Ne in the 2AA's PAS, whereas use of the second set provides the coordinates of Ne in the 2AA-Ne's PAS. Based on the different combinations' signs, eight positions are possible for each set, but only in one case they overlap (see Fig. 5). This overlapping provides a direct indication of the position of the Ne atom above the hydrogen bonded, ring-like structure of 2AA. With regard to other complexes with rare gases, a similar behavior has been observed in the argon complex of guaiacol (or 2-methoxyphenol),³³ where the Ar atom is located above the five membered ring closed by the OH-O HB, instead of the aromatic ring. The distance of neon from the ring plane, given by the c_s coordinate in the PAS of 2AA, is 3.2569(5) Å—a value smaller than those determined for the complexes of other planar compounds such as benzene 3.408 Å,⁵⁰ 2,5-dihydrofuran 3.305 Å,⁵¹ and pentafluoropyridine 3.277 Å.¹³

The nuclear quadrupole coupling constants provide additional independent information on the molecular geometry of the complexes. We see that the χ_{cc} component of 2AA and 2AA-W are equal within the standard errors quoted, and that by rotating the nuclear quadrupole tensor of 2AA by 10.5° around the *c* axis, we can reproduce the values of 2AA-W, achieving $\chi_{aa} = 1.24$ and $\chi_{bb} = 2.56$ MHz. This finding, together with the absence of μ_c -type transition lines

TABLE VI. Experimental substitution coordinates ($r_s/\text{Å}$) and theoretical equilibrium coordinates ($r_e/\text{Å}$, B3LYP-D3(BJ)/def2-TZVP and MP2/aug-cc-pVTZ).

2AA(I)	$ a_s $	$ b_s $	$ c_s $	a_e^{B3LYP}	b_e^{B3LYP}	c_e^{B3LYP}	a_e^{MP2}	b_e^{MP2}	c_e^{MP2}
C1	0.1499(101) ^a	0.2089(72)	0.01(13)	-0.2085	-0.2271	0.0000	-0.2042	-0.2242	-0.0113
C2	0.5438(28)	0.9685(16)	0.05(3)	0.5584	0.9750	0.0000	0.5532	0.9758	-0.0084
C3	1.9638(8)	0.8762(17)	0.04(3)	1.9652	0.8741	0.0000	1.9569	0.8784	0.0117
C4	2.6016(6)	0.3425(44)	$i0.05(3)^b$	2.5931	-0.3500	0.0000	2.5980	-0.3475	0.0199
C5	1.8562(8)	1.5396(10)	$i0.03(6)$	1.8505	-1.5355	0.0000	1.8555	-1.5322	0.0052
C6	0.4666(33)	1.4597(11)	$i0.03(6)$	0.4750	-1.4557	0.0000	0.4734	-1.4571	-0.0097
C7	1.6783(9)	0.1809(84)	0.02(8)	-1.6772	-0.1903	0.0000	-1.6790	-0.1977	0.0065
C8	2.4546(6)	1.4966(11)	0.02(8)	-2.4486	-1.4953	0.0000	-2.4322	-1.5073	-0.0235
N10	$i0.0438(344)$	2.2060(7)	0.03(5)	-0.0280	2.1946	0.0000	-0.0361	2.2082	-0.0663
2AA-H ₂ O(I)	$ a_s $	$ b_s $	$ c_s $	a_e^{B3LYP}	b_e^{B3LYP}	c_e^{B3LYP}	a_e^{MP2}	b_e^{MP2}	c_e^{MP2}
C1	0.3948(40)	0.2454(64)	$i0.08(2)$	0.4156	-0.2710	-0.0108	0.4147	-0.2597	-0.0209
C2	1.0636(15)	0.9928(16)	0.10(2)	1.0693	0.9973	-0.0020	1.0789	0.9949	-0.0095
C3	2.4827(7)	1.0312(17)	0.08(2)	2.4798	1.0254	0.0135	2.4860	1.0037	0.0274
C4	3.2304(5)	0.1342(119)	0.09(2)	3.2168	-0.1352	0.0169	3.2176	-0.1695	0.0449
C5	2.5998(6)	1.3860(11)	$i0.03(6)$	2.5863	-1.3848	0.0053	2.5672	-1.4076	0.0232
C6	1.2130(13)	1.4363(11)	0.02(7)	1.2110	-1.4327	-0.0075	1.1848	-1.4384	-0.0086
C7	1.0297(15)	0.3746(42)	0.06(3)	-1.0438	-0.3771	-0.0148	-1.0530	-0.3522	-0.0244
C8	1.6880(9)	1.7443(9)	$i0.05(3)$	-1.6926	-1.7431	-0.0108	-1.7039	-1.7122	-0.0551
O _{water}	4.6043(3)	0.1304(116)	0.07(2)	-4.5764	0.1615	0.0771	-4.5501	0.0971	0.0743
2AA-Ne(I)	$ a_s $	$ b_s $	$ c_s $	a_e^{B3LYP}	b_e^{B3LYP}	c_e^{B3LYP}	a_e^{MP2}	b_e^{MP2}	c_e^{MP2}
Ne (PAS complex)	1.5124(10)	1.6057(9)	2.0177(7)	-1.3295	1.6044	2.0118	-1.2049	1.5367	2.0259
Ne (PAS monomer)	0.9470(16)	0.6526(23)	3.2569(5)	-0.8757	0.8634	3.0893	-0.8119	0.8529	3.0080

^aCostain error⁴⁹ is reported in units of the last digit.

^bDue to the contribution of the large amplitude motions, coordinates close to zero can assume an imaginary value.

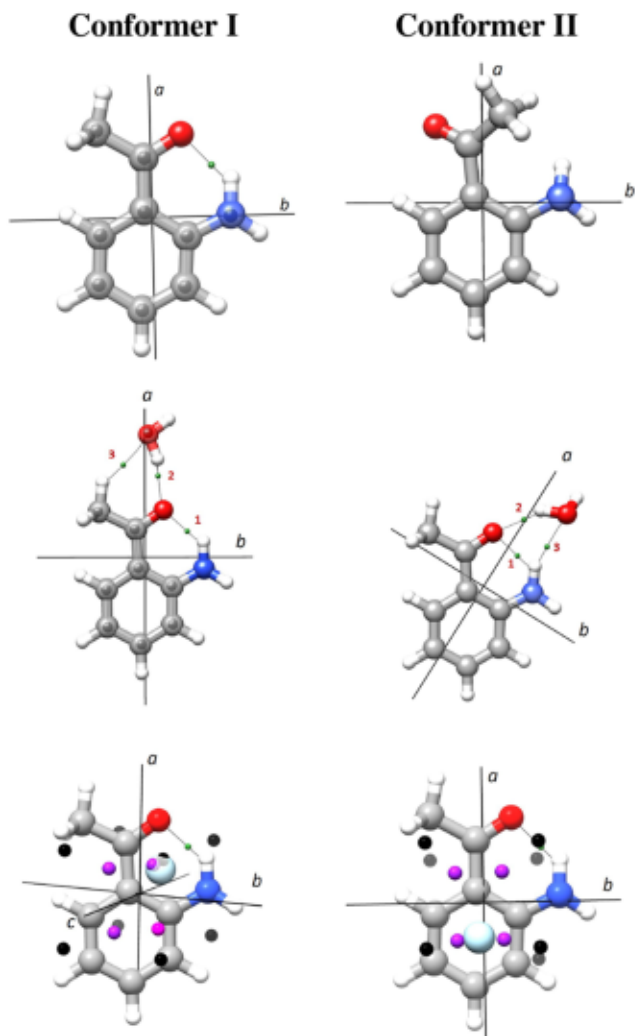


FIG. 5. Computed structures (MP2/aug-cc-pVTZ, ball and stick representation, colored according to the CPK scheme),⁶⁷ principal inertial axes, and intermolecular bond critical points (small green spheres) of 2AA, 2AA-W, and 2AA-Ne. The experimental atoms' positions determined by the isotope substitution method are shown as superimposed black spheres. For the Ne atom, all possible positions are shown for both the PAS of the complex and the monomer (purple spheres), evidencing that the matching position corresponds to the Ne atom above the hydrogen bonded ring.

in the spectrum, suggests that water lies in the symmetry plane of 2AA. This deduction seems to be contradicted by the experimental value of $M_{cc} = 2.2686(1) \text{ u}\text{\AA}^2$ for the complex, which is higher than that of the monomer ($M_{cc} = 1.8040(1) \text{ u}\text{\AA}^2$), and the theoretical results, which locate the free H atom of water definitely out of plane in the case of DFT (HOHC8 = $\pm 114.5^\circ$, $M_{cc} = 2.26 \text{ u}\text{\AA}^2$) and slightly out of plane (HOHC8 = $\pm 164.4^\circ$, $M_{cc} = 1.89 \text{ u}\text{\AA}^2$) in the case of MP2. However, all this information is coherent if we hypothesize that the hydroxyl group undergoes a large amplitude motion above and below the symmetry plane, with the barrier to planarity being so small that the vibrational ground state lies above it.

Actually, the hypothesis is confirmed by the calculated DFT barrier (54.4 cm^{-1}) and the zero point energy related to the hydroxyl torsion (53.7 cm^{-1}), which are of the same magnitude. Moreover, the M_{cc} value is similar to that of monohydrated acetophenone ($2.212(1) \text{ u}\text{\AA}^2$),³⁹ where the C_s symmetry was definitively ascertained by the unchanged value for M_{cc} under substitution of the water free proton with deuterium. All the observations are in agreement with a structure where the intramolecular HB is conserved, and the water molecule lies on the ab plane, keeping the system at the C_s symmetry. Finally, the same planar arrangement has been observed in several monohydrated bidentate complexes, for instance: trifluoroacetophenone,⁵² acrolein,⁵³ trifluoroacetone,⁵⁴ acrylonitrile,⁵⁵ and pyridine analog (diazines,⁵⁶⁻⁵⁸ triazine,⁵⁹ 3-fluoropyridine,⁶⁰ and 2-(trifluoromethyl)pyridine⁶¹).

According to the above considerations, the C–C bond distances were derived from the substitution coordinates of 2AA and 2AA-W, setting the c_s -coordinate to zero. The obtained values are compared to the theoretical ones in Table VII. Regardless of the presence of water, the values obtained for the two species are similar, with differences lying below 1 pm, except for the distances involving the C1 atom. This can reasonably be ascribed to the large uncertainty of the very small C1 a_s coordinate in the PAS of 2AA ($|a_s| = 0.15(1) \text{ \AA}$). However, when water binds to the acetyl group, the center of mass shifts, resulting in a more reliable position of C1 in the PAS of 2AA-W ($|a_s| = 0.395(4) \text{ \AA}$). Neglecting the coordinates of C1 in 2AA, we find that, according to the existence of a resonant zwitterionic structure (Fig. 4), the C3–C4 and C5–C6 bonds are shorter (about 1.39 Å) than the other aromatic C–C bonds (1.40–1.45 Å), and C7–C1 (1.43 Å) is shorter than C8–C7 (1.52 Å) in the alkyl chain.

As for the neon complex, upon complexation, the PAS of 2AA is completely rotated. Nevertheless, it is possible to transform the nuclear quadrupole coupling constants of the monomer into those of 2AA-Ne through the following intrinsic rotation matrix:

$$R = \begin{bmatrix} \cos \gamma & -\sin \gamma & 0 \\ \sin \gamma & \cos \gamma & 0 \\ 0 & 0 & 1 \end{bmatrix} \begin{bmatrix} \cos \beta & 0 & \sin \beta \\ 0 & 1 & 0 \\ -\sin \beta & 0 & \cos \beta \end{bmatrix} \begin{bmatrix} 1 & 0 & 0 \\ 0 & \cos \alpha & -\sin \alpha \\ 0 & \sin \alpha & \cos \alpha \end{bmatrix}, \quad (3)$$

TABLE VII. Experimental (r_s) and theoretical (r_e , B3LYP-D3(BJ)/def2-TZVP and MP2/aug-cc-pVTZ) C–C bond distances (Å).

	r_s		r_e^{B3LYP}		r_e^{MP2}	
	2AA	2AA-W	2AA	2AA-W	2AA	2AA-W
C1–C2	1.367	1.407	1.426	1.427	1.419	1.420
C2–C3	1.422	1.420	1.410	1.411	1.407	1.408
C3–C4	1.376	1.385	1.376	1.375	1.383	1.383
C4–C5	1.410	1.402	1.399	1.400	1.398	1.399
C5–C6	1.392	1.388	1.378	1.376	1.384	1.383
C1–C6	1.394	1.445	1.406	1.408	1.407	1.408
C1–C7	1.528	1.430	1.469	1.463	1.475	1.471
C7–C8	1.528	1.520	1.516	1.512	1.511	1.508

where $\alpha = 27^\circ$, $\beta = 13^\circ$, and $\gamma = 10^\circ$ are the Euler angles⁶² related to a , b , and c , respectively. The achieved values, $\chi_{aa} = 0.98$, $\chi_{bb} = 1.35$, and $\chi_{cc} = 2.33$ MHz, are in very good agreement with those experimentally determined for 2AA·Ne, suggesting that, despite the fact that neon lies on the ring containing the nitrogen atom, the interaction between the two moieties does not alter the electric field gradient, and thus the electron distribution around the nitrogen atom, in agreement with an overall weakness of the interaction itself. Consistently, the values of the centrifugal distortion constants of 2AA·Ne are quite large, one or two orders of magnitude larger than those of 2AA·W.

VII. NON-COVALENT INTERACTIONS

Nowadays, rotational spectroscopy exploits the developments and successes of computational chemistry for a correct interpretation of results. At the same time, spectroscopic data act as a benchmark for the assessment of quantum chemical theories, resulting in a fruitful synergy.

In the present work, 2AA and its complexes are modeled at the B3LYP-D3(BJ)/def2-TZVP and MP2/aug-cc-pVTZ levels of calculation, and the obtained spectroscopic parameters have been successfully used as a starting point for the fitting procedure. Moreover, the predicted geometries are in good agreement with the experimental structures, if we take into account the large amplitude motion effects. Thus, assuming that the chosen methods properly describe our systems, further theoretical analyses can be carried out in order to gain information on the NCIs.

Bader's quantum theory of atoms in molecules (QTAIM) was applied using the MULTIWFN program.²⁶ According to QTAIM, molecular structure is revealed by the stationary points of the electron density function ($\rho(\mathbf{r})$), together with the gradient paths of the electron density that originate and terminate at these points. Since $\rho(\mathbf{r})$ has a maximum at the nuclei, the localization of maxima enables the identification of atomic positions, whereas chemical bonds are defined as saddle points between the maxima; such saddle points are known as bond critical points (BCPs). The intra- and inter-molecular, non-covalent BCPs for 2AA and its water and neon complexes, are shown in Fig. 5, whereas the corresponding $\rho(\mathbf{r})$ values and the bond distances (d) obtained both at the B3LYP-D3(BJ)/def2-TZVP and MP2/aug-cc-pVTZ levels of calculation are given in Table VIII. Assuming that the $\rho(\mathbf{r})$ at a BCP reflects the strength of the bond, Emamian *et al.*⁶³ proposed the following linear relationship between the interaction energy (E_{int}) and $\rho(\mathbf{r})$ at the corresponding BCPs for HBs in neutral compounds:

$$E_{\text{int}}/\text{kcal} \cdot \text{mol}^{-1} = -223.08 \cdot \rho + 0.7423. \quad (4)$$

The resulting values from this equation are also given in Table VIII. The intramolecular HB (NH-OC) seems to be not altered upon complexation with neon, and only slightly affected by the interaction of water with the acetyl group. On the contrary, more evident weakening takes place when water interacts with the OC7C1C2NH frame (conformer II). In both cases, the intermolecular OH-OC HB is weaker than the intramolecular HB. With regard to the secondary stabilizing interaction involving the water oxygen, it is more effective toward the amino hydrogen atoms (conformer II, HO-HN) instead of the methyl ones (conformer I, HO-HC).

TABLE VIII. Theoretical (B3LYP-D3(BJ)/def2-TZVP and MP2/aug-cc-pVTZ) HB distances ($d/\text{\AA}$), electron density at the corresponding BCPs ($\rho/\text{me} \cdot \text{a}_0^{-3}$), and interaction energies ($E_{\text{int}}/\text{kJ} \cdot \text{mol}^{-1}$).

		d^{B3LYP}	ρ^{B3LYP}	$E_{\text{int}}^{\text{B3LYP}}$	d^{MP2}	ρ^{MP2}	$E_{\text{int}}^{\text{MP2}}$
2AA(I)	NH-OC	1.873	33.8	-28.4	1.888	31.2	-26.0
2AA-Ne(I)	NH-OC	1.872	33.8	-28.4	1.886	31.3	-26.1
2AA-Ne(II)	NH-OC	1.873	33.8	-28.4	1.888	31.2	-26.1
2AA-W(I)	NH-OC	1.882	33.0	-27.7	1.896	30.6	-25.7
2AA-W(II)	NH-OC	2.009	25.5	-20.7	1.999	24.6	-19.9
2AA-W(I)	OH-OC	1.884	28.9	-23.9	1.889	27.2	-22.3
2AA-W(II)	OH-OC	1.942	22.5	-17.9	1.951	20.6	-16.1
2AA-W(I)	HO-HC	2.540	8.7	-5.0	2.449	8.1	-4.5
2AA-W(II)	HO-HN	2.260	12.5	-8.5	2.282	10.5	-6.7

Super-molecular methods can be used to quantify the energy involved in the NCIs. The simplest approach is subtractive, the intermolecular binding energy (D_e) is estimated as the difference between the energy of the binary molecular complex ($A-B$) and the energy of the two constituting units (A and B) in their minimum configuration,

$$D_e = (E_{A-B}) - (E_A + E_B). \quad (5)$$

In a similar way, the interaction energy is achieved as the difference between the energy of the molecular complex and the energy of the isolated monomers in the geometry of the complex (A^* and B^*),

$$E_{\text{int}} = (E_{A-B}) - (E_{A^*} + E_{B^*}). \quad (6)$$

The resulting values given in Table IX, show that the D_e for the dissociation of the 2AA·W complex is about ten times that of the dissociation of the 2AA·Ne one. Moreover, the D_e values are higher for species I than species II, in agreement with the observed conformational preference for conformer I. For neon complexes, E_{int} and D_e are equal, whereas for water complexes, E_{int} is larger than D_e . This further confirms that a structural relaxation upon complexation occurs in water complexes, not in neon complexes. The difference between D_e and E_{int} is proportional to the extent of structural changes, being 0.7–0.8 $\text{kJ} \cdot \text{mol}^{-1}$ in the case of conformer I, where water inserts into the acetyl group without disrupting the intramolecular HB, and 2.2 $\text{kJ} \cdot \text{mol}^{-1}$ in conformer II, where water interferes with the intramolecular HB.

A different approach is provided by SAPT, which considers the total interaction energy as a perturbation to the total system energy.²⁷ An advantage of this method with respect to the subtractive one is that the interaction energy is made free of the basis set superposition error in a natural way. We used a higher order SAPT approach (DF-SAPT2+(3) δ MP2/aug-cc-pVTZ) implemented in the PSI4 package,²⁸ obtaining the E_{int} values given in Table IX, with their electrostatic, exchange-repulsion, induction, and dispersion components. Compared to the subtractive method, the SAPT interaction energies of water complexes, are similar to the MP2/aug-cc-pVTZ and smaller than the B3LYP-D3(BJ)/def2-TZVP values. We also note that the main stabilizing contribution is electrostatic. Differently, for what concerns the neon complexes, the SAPT estimated

TABLE IX. Theoretical binding and interaction energies ($\text{kJ}\cdot\text{mol}^{-1}$). The exchange–repulsion, induction and dispersion components obtained with the SAPT approach are also given.

	2AA-W(I)	2AA-W(II)	2AA-Ne(I)	2AA-Ne(II)
B3LYP-D3(BJ)/def2-TZVP				
D_e	-31.62	-28.99	-3.13	-2.99
E_{int}	-32.37	-31.21	-3.13	-2.98
MP2/aug-cc-pVTZ				
D_e	-27.88	-25.52	-3.91	-3.82
E_{int}	-28.56	-27.19	-3.92	-3.83
DF-SAPT2+(3) δ MP2/aug-cc-pVTZ//MP2/aug-cc-pVTZ				
E_{int}	-27.45	-25.24	-2.03	-1.79
Electrostatic	-44.58	-37.64	-1.05	-1.53
Exch.-repulsion	+51.93	+41.43	+3.56	+4.97
Induction	-16.43	-11.54	-0.09	-0.13
Dispersion	-18.37	-17.49	-4.45	-5.10

interaction energies are the smallest ones and the main stabilizing contribution is dispersion.

VIII. CONCLUSIONS

To our knowledge, this is the first rotational spectroscopy study on 2AA. It clearly indicates that, for the isolated system in the gas phase, the strong intramolecular RAHB interaction between the carbonyl and the amino groups dominates the structural features. Indeed, an overall stiffening of the torsional modes of the phenyl substituents is produced, leading to a C_s geometry, which is consistent with the formation of an aromatic bicyclic-like system, not easily breakable. Accordingly, complexation with water takes place at the acetyl end, preventing the weakening of the intramolecular HB, and the Ne atom binds to the NCI closed ring. An analogous behavior was found in the anthranilic acid, where water binds to the carboxyl group, having little effect on the NH-O bond.⁴⁷ Differently, in the condensed phase, the participation of other interaction forces can lead to a non-planar shape of the molecule. This has been found in the x-ray crystal structure of kynurenine formamidase from *Bacillus anthracis* complexed with 2AA,⁶⁴ where the OC7C1C2 torsion angle is 35° . Generally speaking, it is well known that the interactions with receptors are a balance between the cost of disrupting the isolated structure and the gain from the intermolecular NCIs. In this sense, the behavior of 2AA can be considered opposite to that of 2-aminoethanol. Indeed, due to the reduced length of the alkyl chain, the intramolecular hydrogen bond constrains 2-aminoethanol to a high energy, folded arrangement. In this case, the insertion of a bridged ligand between the hydroxyl and amino groups allows for a structural relaxation, as has been shown by the rotational spectroscopy studies on water⁶⁵ and ammonia⁶⁶ complexes. Overall, this study, together with the cited examples, shows that the stability of a molecular system is determined by the balance of several forces, whose effects can be disentangled combining spectroscopic and quantum mechanical methods.

SUPPLEMENTARY MATERIAL

See the [supplementary material](#) for the theoretical molecular coordinates and the experimental rotational transition frequencies.

ACKNOWLEDGMENTS

S.B. and J.C.L. acknowledge the Junta de Castilla y León (Grant No. INFRARED-FEDER IR2020-1-UVa02) the Ministerio de Economía y Competitividad (Grant No. CTQ2016-75253-P), and the Ministerio de Ciencia e Innovación (Grant No. PID2021-125207NB-C33). S.M., L.E., and A.M. acknowledge the Italian MIUR (Attività Base di Ricerca), the University of Bologna (Ricerca Fondamentale Orientata), the CINECA award under the ISCRA initiative for providing high-performance computing resources and support, and the author community of REVTEX.

AUTHOR DECLARATIONS

Conflict of Interest

The authors have no conflicts to disclose.

Author Contributions

G. Salvitti: Conceptualization (equal); Data curation (equal); Formal analysis (lead); Investigation (lead); Visualization (lead); Writing – original draft (equal); Writing – review & editing (equal). **S. Blanco:** Conceptualization (equal); Data curation (equal); Formal analysis (equal); Funding acquisition (equal); Investigation (lead); Resources (equal); Supervision (lead); Validation (equal); Visualization (supporting); Writing – review & editing (equal). **J. C. López:** Conceptualization (equal); Data curation (equal); Formal analysis (equal); Funding acquisition (equal); Investigation (equal); Resources (equal); Supervision (equal); Validation (equal); Visualization (supporting); Writing – review & editing (equal). **S. Melandri:** Conceptualization (equal); Data curation (equal); Formal analysis (equal); Funding acquisition (equal); Investigation (equal); Resources (equal); Supervision (equal); Validation (equal); Visualization (supporting); Writing – review & editing (equal). **L. Evangelisti:** Conceptualization (equal); Data curation (equal); Formal analysis (equal); Funding acquisition (equal); Investigation (equal); Resources (equal); Supervision (equal); Validation (equal); Visualization (supporting); Writing – review & editing (equal). **A. Maris:** Conceptualization (lead); Data curation (lead); Formal analysis (lead); Funding acquisition (equal); Investigation (lead); Resources (equal); Supervision (lead); Validation (equal); Visualization (equal); Writing – original draft (lead); Writing – review & editing (equal).

DATA AVAILABILITY

The data that support the findings of this study are available within the article and its [supplementary material](#).

REFERENCES

- G. G. Brown, B. C. Dian, K. O. Douglass, S. M. Douglass, S. T. Shipman, and B. H. Shipman, "A broadband Fourier transform microwave spectrometer based on chirped pulse excitation," *Rev. Sci. Instrum.* **79**, 053103 (2008).
- Q. Sun, M. J. Gates, E. H. Lavin, T. E. Acree, and G. L. Sacks, "Comparison of odor-active compounds in grapes and wines from *Vitis vinifera* and

- non-foxy American grape species," *J. Agric. Food Chem.* **59**, 10657–10664 (2011).
- ³K. Hoenicke, T. J. Simat, H. Steinhart, N. Christoph, M. Gefner, and H.-J. Köhler, "Unusual aging off-flavor in wine: formation of 2-aminoacetophenone and evaluation of its influencing factors," *Anal. Chim. Acta* **458**, 29–37 (2002).
- ⁴A. Rapp, G. Versini, and H. Ullemeyer, "2-aminoacetophenone: Causal component of 'unusual aging flavour' ('naphthalene note,' 'hybrid note') of wine," *Vitis* **32**, 61–62 (1993).
- ⁵O. W. Parks, D. P. Schwartz, and M. Keeney, "Identification of o-aminoacetophenone as a flavour compound in stale dry milk," *Nature* **202**, 185–187 (1964).
- ⁶S. McLean, D. S. Nichols, and N. W. Davies, "Volatile scent chemicals in the urine of the red fox, *Vulpes vulpes*," *PLoS One* **16**, e0248961 (2021).
- ⁷J. X. Zhang, H. A. Soini, K. E. Bruce, D. Wiesler, S. K. Woodley, M. J. Baum, and M. V. Novotny, "Putative chemosignals of the ferret (*Mustela furo*) associated with individual and gender recognition," *Chem. Senses* **30**, 727–737 (2005).
- ⁸R. E. Page, M. S. Blum, and H. M. Fales, "o-aminoacetophenone, a pheromone that repels honeybees (*Apis mellifera* L.)," *Experientia* **44**, 270–271 (1988).
- ⁹S. E. Kapsetaki, I. Tzelepis, K. Avgousti, I. Livadaras, N. Garantonakis, K. Varikou, and Y. Apidianakis, "The bacterial metabolite 2-aminoacetophenone promotes association of pathogenic bacteria with flies," *Nat. Commun.* **5**, 4401 (2014).
- ¹⁰A. J. Scott-Thomas, M. Syhre, P. K. Pattemore, M. Epton, R. Laing, J. Pearson, and S. T. Chambers, "2-aminoacetophenone as a potential breath biomarker for *Pseudomonas aeruginosa* in the cystic fibrosis lung," *BMC Pulm. Med.* **10**, 56 (2010).
- ¹¹A. P. Horsfield, A. Haase, and L. Turin, "Molecular recognition in olfaction," *Adv. Phys. X* **2**, 937–977 (2017).
- ¹²S. E. Wheeler and J. W. G. Bloom, "Toward a more complete understanding of noncovalent interactions involving aromatic rings," *J. Phys. Chem. A* **118**, 6133–6147 (2014).
- ¹³A. Macario, S. Blanco, I. Alkorta, and J. C. López, "Perfluorination of aromatic compounds reinforce their van der Waals interactions with rare gases: The rotational spectrum of pentafluoropyridine-Ne," *Molecules* **27**, 17 (2022).
- ¹⁴P. Pinacho, S. Blanco, and J. C. López, "The complete conformational panorama of formamide–water complexes: The role of water as a conformational switch," *Phys. Chem. Chem. Phys.* **21**, 2177–2185 (2019).
- ¹⁵Z. Kisiel, L. Pszczółkowski, I. R. Medvedev, M. Winniewisser, F. C. De Lucia, and E. Herbst, "Rotational spectrum of *trans-trans* diethyl ether in the ground and three excited vibrational states," *J. Mol. Spectrosc.* **233**, 231–243 (2005).
- ¹⁶Z. Kisiel, "Prospe-programs for rotational spectroscopy," <http://info.ifpan.edu.pl/~kisiel/prospe.htm/>; accessed 08 April 2022.
- ¹⁷H. M. Pickett, *J. Mol. Spectrosc.* **148**, 371–377 (1991).
- ¹⁸Gaussian is a registered trademark of Gaussian, Inc., 340 Quinipiac St. Bldg., Wallingford, CT 06492 USA, 40.
- ¹⁹A. D. Becke, "Density-functional thermochemistry. III. The role of exact exchange," *J. Chem. Phys.* **98**, 5648–5652 (1993).
- ²⁰C. Lee, W. Yang, and R. G. Parr, "Development of the Colle-Salvetti correlation-energy formula into a functional of the electron density," *Phys. Rev. B* **37**, 785–789 (1988).
- ²¹S. Grimme, J. Antony, S. Ehrlich, and H. Krieg, "A consistent and accurate *ab initio* parametrization of density functional dispersion correction (DFT-D) for the 94 elements H–Pu," *J. Chem. Phys.* **132**, 154104 (2010).
- ²²S. Grimme, S. Ehrlich, and L. Goerigk, "Effect of the damping function in dispersion corrected density functional theory," *J. Comput. Chem.* **32**, 1456 (2011).
- ²³F. Weigend and R. Ahlrichs, "Balanced basis sets of split valence, triple zeta valence and quadruple zeta valence quality for H to Rn: Design and assessment of accuracy," *Phys. Chem. Chem. Phys.* **7**, 3297–3305 (2005).
- ²⁴C. Møller and M. S. Plesset, "Note on an approximation treatment for many-electron systems," *Phys. Rev.* **46**, 618–622 (1934).
- ²⁵T. H. Dunning, "Gaussian basis sets for use in correlated molecular calculations. I. The atoms boron through neon and hydrogen," *J. Chem. Phys.* **90**, 1007–1023 (1989).
- ²⁶T. Lu and F. Chen, "Multiwfn: A multifunctional wavefunction analyzer," *J. Comput. Chem.* **33**, 580–592 (2012).
- ²⁷B. Jeziorski, R. Moszynski, and K. Szalewicz, "Perturbation theory approach to intermolecular potential energy surfaces of van der Waals complexes," *Chem. Rev.* **94**, 1887–1930 (1994).
- ²⁸R. M. Parrish, L. A. Burns, D. G. A. Smith, A. C. Simmonett, A. E. DePrince, E. G. Hohenstein, U. Bozkaya, A. Y. Sokolov, R. Di Remigio, R. M. Richard, J. P. Gonthier, A. M. James, H. R. McAlexander, A. Kumar, M. Saitow, X. Wang, B. P. Pritchard, P. Verma, H. F. Schaefer, K. Patkowski, R. A. King, E. F. Valeev, F. A. Evangelista, J. M. Turney, T. D. Crawford, and C. D. Sherrill, "Psi4 1.1: An open-source electronic structure program emphasizing automation, advanced libraries, and interoperability," *J. Chem. Theory Comput.* **13**, 3185–3197 (2017).
- ²⁹Z. Kisiel, "A simple model for predicting structures of gas-phase van der Waals dimers containing a rare-gas atom," *J. Phys. Chem.* **95**, 7605–7612 (1991).
- ³⁰J. C. López, A. Macario, and S. Blanco, "Conformational equilibria in o-anisic acid and its monohydrated complex: The prevalence of the *trans*-COOH form," *Phys. Chem. Chem. Phys.* **21**, 6844–6850 (2019).
- ³¹A. Macario, S. Blanco, J. Thomas, Y. Xu, and J. C. López, "Competition between intra- and intermolecular hydrogen bonding: o-anisic acid–formic acid heterodimer," *Chem. Eur. J.* **25**, 12325–12331 (2019).
- ³²S. Blanco, A. Maris, S. Melandri, and W. Caminati, "Rotational spectrum of propylene oxide–neon," *Mol. Phys.* **100**, 3245–3249 (2002).
- ³³R. M. Gurusinge, A. Fox-Loe, and M. J. Tubergen, "Structures of guaiacol and the guaiacol–argon van der Waals complex from rotational spectroscopy of guaiacol isotopologues," *J. Mol. Struct.* **1246**, 131233 (2021).
- ³⁴J. Watson, *Vibrational Spectra and Structure* (Elsevier, New York, 1977).
- ³⁵G. Di Modica, L. Evangelisti, L. Foschini, A. Maris, and S. Melandri, "Testing the scalability of the HS-AUTOFIT tool in a high-performance computing environment," *Electronics* **10**, 2251 (2021).
- ³⁶B. S. Ray, "Über die eigenwerte des asymmetrischen kreisels," *Z. Phys.* **78**, 74–91 (1932).
- ³⁷E. Ye, K. Chandrasekaran, and R. P. Bettens, "Millimeter wave measurement and assignment of the rotational spectrum of aniline," *J. Mol. Spectrosc.* **229**, 54–56 (2005).
- ³⁸M. Onda, Y. Kohama, K. Suga, and I. Yamaguchi, "Microwave spectrum and molecular planarity of acetophenone," *J. Mol. Struct.* **442**, 19–22 (1998).
- ³⁹J. Lei, J. Zhang, G. Feng, J.-U. Grabow, and Q. Gou, "Conformational preference determined by inequivalent n-pairs: Rotational studies on acetophenone and its monohydrate," *Phys. Chem. Chem. Phys.* **21**, 22888–22894 (2019).
- ⁴⁰J. Durig, H. Bist, K. Furic, J. Qiu, and T. Little, "Far infrared spectra and barriers to internal rotation of benzaldehyde, benzoyl fluoride, benzoyl chloride and acetophenone," *J. Mol. Struct.* **129**, 45–56 (1985).
- ⁴¹See <https://webbook.nist.gov/> for the gas phase infrared spectra of aniline and 2'-aminoacetophenone; accessed 08 April 2022.
- ⁴²F. J. Lovas, R. D. Suenram, G. T. Fraser, C. W. Gillies, and J. Zozom, "The microwave spectrum of formamide–water and formamide–methanol complexes," *J. Chem. Phys.* **88**, 722–729 (1988).
- ⁴³S. Blanco, J. C. López, A. Lesarri, and J. L. Alonso, "Microsolvation of formamide: A rotational study," *J. Am. Chem. Soc.* **128**, 12111–12121 (2006).
- ⁴⁴R. B. Corey, L. C. Pauling, and W. T. Astbury, "Fundamental dimensions of polypeptide chains," *Proc. R. Soc. B* **141**, 10–20 (1953).
- ⁴⁵G. Gilli, F. Bellucci, V. Ferretti, and V. Bertolasi, "Evidence for resonance-assisted hydrogen bonding from crystal-structure correlations on the enol form of the β -diketone fragment," *J. Am. Chem. Soc.* **111**, 1023–1028 (1989).
- ⁴⁶C. A. Southern, D. H. Levy, G. M. Florio, A. Longarte, and T. S. Zwier, "Electronic and infrared spectroscopy of anthranilic acid in a supersonic jet," *J. Phys. Chem. A* **107**, 4032–4040 (2003).
- ⁴⁷J. A. Stearns, A. Das, and T. S. Zwier, "Hydrogen atom dislocation in the excited state of anthranilic acid: Probing the carbonyl stretch fundamental and the effects of water complexation," *Phys. Chem. Chem. Phys.* **6**, 2605–2610 (2004).
- ⁴⁸S. Leśniewski, P. Kolek, K. Pirowska, A. L. Sobolewski, and J. Najbar, "Franck–Condon analysis of laser-induced fluorescence excitation spectrum of anthranilic acid: Evaluation of geometry change upon $S_0 \rightarrow S_1$ excitation," *J. Chem. Phys.* **130**, 054307 (2009).
- ⁴⁹J. Kraitchman, "Determination of molecular structure from microwave spectroscopic data," *Am. J. Phys.* **21**, 17–25 (1953).

- ⁵⁰E. Arunan, T. Emilsson, and H. S. Gutowsky, "Rotational spectra and structures of Rg-C₆H₆-H₂O trimers and the Ne-C₆H₆ dimer (Rg = Ne, Ar, or Kr)," *J. Chem. Phys.* **101**, 861–868 (1994).
- ⁵¹A. Maris, P. G. Favero, A. Dell'Erba, and W. Caminati, "Complexes of neon with nonaromatic ring molecules: Rotational spectrum, dynamics, and bond energy of 2,5-dihydrofuran–neon," *J. Chem. Phys.* **110**, 8976–8979 (1999).
- ⁵²J. Lei, S. Alessandrini, J. Chen, Y. Zheng, L. Spada, Q. Gou, C. Puzzarini, and V. Barone, "Rotational spectroscopy meets quantum chemistry for analyzing substituent effects on non-covalent interactions: The case of the trifluoroacetophenone–water complex," *Molecules* **25**, 4899 (2020).
- ⁵³W. Li, A. Maris, C. Calabrese, I. Usabiaga, W. D. Geppert, L. Evangelisti, and S. Melandri, "Atmospherically relevant acrolein–water complexes: Spectroscopic evidence of aldehyde hydration and oxygen atom exchange," *Phys. Chem. Chem. Phys.* **21**, 23559–23566 (2019).
- ⁵⁴L. B. Favero, L. Evangelisti, A. Maris, A. Vega-Toribio, A. Lesarri, and W. Caminati, "How trifluoroacetone interacts with water," *J. Phys. Chem. A* **115**, 9493–9497 (2011).
- ⁵⁵C. Calabrese, A. Vigorito, A. Maris, S. Mariotti, P. Fathi, W. D. Geppert, and S. Melandri, "Millimeter wave spectrum of the weakly bound complex CH₂=CHCN·H₂O: Structure, dynamics, and implications for astronomical search," *J. Phys. Chem. A* **119**, 11674–11682 (2015).
- ⁵⁶S. Melandri, M. E. Sanz, W. Caminati, P. G. Favero, and Z. Kisiel, "The hydrogen bond between water and aromatic bases of biological interest: An experimental and theoretical study of the 1:1 complex of pyrimidine with water," *J. Am. Chem. Soc.* **120**, 11504–11509 (1998).
- ⁵⁷W. Caminati, L. B. Favero, P. G. Favero, A. Maris, and S. Melandri, "Intermolecular hydrogen bonding between water and pyrazine," *Angew. Chem., Int. Ed.* **37**, 792–795 (1998).
- ⁵⁸W. Caminati, P. Moreschini, and P. G. Favero, "The hydrogen bond between water and aromatic bases of biological interest: Rotational spectrum of pyridazine–water," *J. Phys. Chem. A* **102**, 8097–8100 (1998).
- ⁵⁹A. Maris, S. Melandri, M. Miazzi, and F. Zerbetto, "Interactions of aromatic heterocycles with water: The driving force from free-jet rotational spectroscopy and model electrostatic calculations," *ChemPhysChem* **9**, 1303–1308 (2008).
- ⁶⁰C. Calabrese, Q. Gou, L. Spada, A. Maris, W. Caminati, and S. Melandri, "Effects of fluorine substitution on the microsolvation of aromatic azines: The microwave spectrum of 3-fluoropyridine–water," *J. Phys. Chem. A* **120**, 5163–5168 (2016).
- ⁶¹X. Li, Y. Zheng, Q. Gou, G. Feng, and Z. Xia, "Microwave spectroscopy of 2-(trifluoromethyl)pyridine–water complex: Molecular structure and hydrogen bond," *J. Chem. Phys.* **148**, 044306 (2018).
- ⁶²W. Gordy and R. Cook, in *Microwave Molecular Spectra*, edited by A. Weissberger (Wiley, New York, 1984).
- ⁶³S. Emamian, T. Lu, H. Kruse, and H. Emamian, "Exploring nature and predicting strength of hydrogen bonds: A correlation analysis between atoms-in-molecules descriptors, binding energies, and energy components of symmetry-adapted perturbation theory," *J. Comput. Chem.* **40**, 2868–2881 (2019).
- ⁶⁴L. Díaz-Sáez, V. Srikannathasan, M. Zoltner, and W. N. Hunter, "Structures of bacterial kynurenine formamidase reveal a crowded binuclear zinc catalytic site primed to generate a potent nucleophile," *Biochem. J.* **462**, 581–589 (2014).
- ⁶⁵M. J. Tubergen, C. R. Torok, and R. J. Lavrich, "Effect of solvent on molecular conformation: Microwave spectra and structures of 2-aminoethanol van der Waals complexes," *J. Chem. Phys.* **119**, 8397–8403 (2003).
- ⁶⁶S. Melandri, A. Maris, and L. Favero, "The double donor/acceptor role of the NH₃ group: Microwave spectroscopy of the aminoethanol–ammonia molecular complex," *Mol. Phys.* **108**, 2219–2223 (2010).
- ⁶⁷W. L. Koltun, "Space filling atomic units and connectors for molecular models," Patent number US-3170246-A, <http://patft.uspto.gov/netacgi/nph-Parser?Sect1=PTO1&Sect2=HITOFF&p=1&u=/netahtml/PTO/srchnum.html&r=1&f=G&l=50&d=PALL&s1=3170246.PN><https://patents.google.com/patent/US3170246A>.
- ⁶⁸C. C. Costain, "Determination of molecular structures from ground state rotational constants," *J. Chem. Phys.* **29**, 864–874 (1958).